Ain Shams Engineering Journal (2016) xxx, xxx–xxx

Ain Shams University

Ain Shams Engineering Journal

www.elsevier.com/locate/asej
www.sciencedirect.com

ENGINEERING PHYSICS AND MATHEMATICS

Numerical study of heat transfer enhancement in MHD free convection flow over vertical plate utilizing nanofluids

Siva Reddy Sheri [a,*], Thirupathi Thumma [b]

[a] Department of Mathematics, GITAM University, Hyderabad Campus, Medak 502329, Telangana, India
[b] Department of Mathematics, BVRIT, Narsapur, Medak 502313, Telangana, India

Received 9 January 2016; revised 20 June 2016; accepted 30 June 2016

KEYWORDS

Magnetohydrodynamic;
Nanofluid;
Viscous dissipation;
Radiation;
Finite Element Method

Abstract A comprehensive numerical study of heat transfer enhancement in MHD free convection flow over vertical plate utilizing nanofluids has been carried out. Problem is formulated by using nanofluid volume fraction model by considering water based nanofluids containing copper and aluminum oxide. The transformed coupled, nonlinear dimensionless partial differential equations are solved numerically by using finite element method. The influence of pertinent physical parameters on velocity and temperature profiles is discussed and depicted with the aid of graphs. Finally, the numerical values of skin friction and Nusselt number within the flow regime are compared with the previously published work to ensure the correctness of this numerical scheme and an excellent agreement is obtained.

1. Introduction

The term "Nanofluid" describes a colloidal mixture containing ultra-fine particles called as nanoparticles and it is initially coined by Choi [1,2]. In his works he showed that a very small amount of guest nanoparticles, when dispersed uniformly and suspended stably in host fluids, can provide substantial improvements in the thermal properties of base fluids. Nanofluids are engineered by suspending nanoparticles (Cu, Al, Al_2O_3, TiO_2, SiC, SiN, AlN) with average sizes less than 100 nm in conventional heat transfer fluids (H_2O, $C_2H_6O_2$) and also other base fluids such as engine oil, mineral oil, bio-fluids and poor heat transfer fluids. During the past decade the study of thermal properties of nanofluids has attracted immense enthusiasm from research in view of its remarkable applications in electronics, optical devices, material synthesis, high power x-rays, lasers and biomedical sciences. The unsteady vertical motion of a soluble particle in Newtonian media is investigated by Hatami and Domairry [3]. The problem of nano-liquid film flow and heat transfer over an unsteady stretching surface is comprehensively analyzed by Ahmadi et al. [4]. Hatami and Ganji [5] studied the radial position and phase plane of a spherical particle on a rotating parabolic surface through an analytical approach called multi-step

* Corresponding author.
E-mail address: sreddy7@yahoo.co.in (S.R. Sheri).
Peer review under responsibility of Ain Shams University.

ELSEVIER Production and hosting by Elsevier

http://dx.doi.org/10.1016/j.asej.2016.06.015

Please cite this article in press as: Sheri SR, Thumma T, Numerical study of heat transfer enhancement in MHD free convection flow over vertical plate utilizing nanofluids, Ain Shams Eng J (2016), http://dx.doi.org/10.1016/j.asej.2016.06.015

Nomenclature

B_0	constant applied magnetic field
E	applied electric field
F	thermal radiation
g	acceleration due to gravity
K	permeability parameter
k	permeability of porous medium
k^*	mean absorption coefficient
M	dimensionless magnetic field parameter
C_f	skin friction coefficient
Nu	Nusselt number
Pr	Prandtl number
Q	non-dimensional heat source parameter
Q_H	dimensional heat source
q_r	radiative heat flux
q_w	heat flux from the plate
R	dimensional rotational parameter
S	suction parameter
T	local temperature of the nanofluid
Ec	Eckert number
T_w	wall temperature of the fluid
T_∞	temperature of the ambient nanofluid
U_0	characteristic velocity
w_0	normal velocity
(x, y, z)	Cartesian coordinates
(u, v, w)	velocity component along x, y, and z axes

Greek symbols

α	thermal diffusivity
α_f	thermal diffusivity of the fluid
α_{nf}	thermal diffusivity of the nanofluid
β	thermal expansion coefficient
β_f	coefficient of thermal expansion of the fluid
β_s	coefficient of thermal expansion of the solid
ρ_f	density of the fluid friction
ρ_s	density of the solid friction
ρ_{nf}	density of the nanofluid
v	kinematic viscosity
v_f	kinematic viscosity of the fluid
μ	dynamic viscosity
μ_{nf}	viscosity of the nanofluid
σ	electrical conductivity of the fluid
σ_{nf}	electrical conductivity of the nanofluid
σ^*	Stefan–Boltzmann constant
$(\rho C_p)_{nf}$	heat capacitance of the nanofluid
ε	small constant quantity
θ	non-dimensional temperature

Subscripts

f	fluid
s	solid
nf	nanofluid
w	condition at the wall
∞	condition at free stream

differential transform method (MS-DTM). Recently Rahimi-Gorji et al. [6] investigated the heat transfer and fluid flow analysis for a nanofluid in a fin shaped micro channel heat sink (MCHS) and they used that responsive surface methodology (RSM) to optimize geometry of MCHS. Ghasemi et al. [7] studied the third grade Non-Newtonian (blood) containing nanoparticles through porous arteries in the presence of magnetic field analytically and numerically. Nanofluid flow and heat transfer between two parallel plates with Brownian motion effects are investigated by Sheikholeslami and Ganji [8] by employing (Koo-Kleinstreuer-Li) KKL model. The convective heat transport in nanofluid was investigated by Buongiorno [9] with two phase model and is used by several researchers. However in this paper nanofluid model proposed by Tiwari and Das [10] is envisioned.

Convective heat transfer has been studied extensively in the recent years owing to its wide range of applications of various disciplines in Engineering, Science and Technology. These applications include the solar energy collector performance enhancement with nanofluids, the extraction of geothermal energy, food processing and storage, thermal insulation of buildings, the design of pebble bed nuclear reactors and many more. Hatami and Ganji [11] investigated the problem of natural convection of sodium-aligate Non-Newtonian nanofluid flow between two vertical plates by employing Least Square Method (LSM) and Differential Transform Method (DTM). Magnetic field effects on natural convection of nanofluids with Brownian motion effects are investigated by Sheikholeslami and Ellahi [12]. Non-similar solution for natural convective boundary layer flow over a sphere was embedded in a porous medium saturated with a nanofluid reported by Chamkha et al. [13]. Very recently heat transfer enhancement of nanofluid flow and entropy generation in square enclosures containing a rectangular heated body is studied by Sheikholeslami et al. [14]. Furthermore the detailed reviews on convective transport in nanofluids have been presented in the text books by Nield and Bejan [15].

The magnetohydrodynamic (MHD) flow and heat transfer in porous medium have gained interest due to the effect of magnetic field on boundary-layer in rotating system. This flow attracted many researchers in view of its broad range of applications which include exothermic chemical reactions, underground disposal of radioactive waste material and many more. Furthermore various researchers investigated the effects of ferrohydrodynamics (FHD) and electrohydrodynamics (EHD) in heat and fluid flow problems. Ferrofluid forced convection heat transfer in a semi annulus lid under the influence of variable magnetic field with FHD and MHD effects is studied by Sheikholeslami et al. [16]. Chamkha and Aly [17] reported MHD free convective flow of a nanofluid past a vertical plate in the presence of heat generation or absorption effects. Sheikholeslami et al. [18] investigated magnetic field effect on nanofluid flow and heat transfer in a semi-annulus enclosure by considering the effects of thermophoresis and Brownian motion to get the gradient of nanoparticles volume fraction. Ghasemi et al. [19] analyzed EHD flow in a circular

Please cite this article in press as: Sheri SR, Thumma T, Numerical study of heat transfer enhancement in MHD free convection flow over vertical plate utilizing nanofluids, Ain Shams Eng J (2016), http://dx.doi.org/10.1016/j.asej.2016.06.015

cylindrical conduit by adopting LSM. Effects of spatially variable magnetic field on ferrofluid flow and heat transfer considering constant heat flux boundary conditions are reported by Sheikholeslami [20]. Ellahi [21] studied the effects of MHD and temperature dependent viscosity on the flow of non-Newtonian nanofluid in a pipe. Recently electric filed effects on nanofluid forced convective heat transfer in an enclosure with sinusoidal wall are presented by Sheikholeslami et al. [22]. Unsteady MHD free convection flows past a vertical permeable flat plate in a rotating frame of reference with constant heat source in a nanofluid studied by Hamad and Pop [23]. In addition to the heat transfer effects in a lid driven semi annulus enclosure is studied in the presence of non-uniform magnetic field by Sheikholeslami et al. [24,25]. Furthermore hydrothermal effects in engineering problems by adopting control volume Finite Element Method (CVFEM) have been explained in detail in the text book by Sheikholeslami and Ganji [26].

The Radiation effect on heat transfer problems has received much attention from the last several years due to its broad range of space technology and industrial applications such as glass production, furnace design, gas turbine missiles, plasma physics nuclear power plant, aircrafts and many other possible areas involving high temperatures. Thermal radiation effects of MHD nanofluid flow between two horizontal rotating plates with Brownian motion and thermophoresis effects are studied by Sheikholeslami et al. [27]. Arpaci [28] analyzed the effect of radiation on the laminar free convection from a heated vertical plate. Chamkha [29] studied the radiation effects on mixed convection over a wedge with a nanofluid, over moving surface in a fluid flow studied by Olanrewaju et al. [30], and also an increase in convective heat transfer with increasing nano particle concentration was also reported in the numerical works of Arefmanesh and Mahmoodi [31]. MHD free convection flow of Alumina-water nanofluid considering thermal radiation in an enclosure with a constant heat flux is reported by Sheikholeslami et al. [32].

Viscosity has got a lot of importance due to its potential applications like the pumping power is related to the viscosity of a fluid, in laminar flow the pressure drop is directly proportional to the viscosity and convective heat transfer coefficient is influenced by viscosity. Domairry and Hatami [33] studied the effects of squeezing film of Cu-water nanofluid between parallel plates using DTM method. Siva Reddy and Srinivasa [34] have studied Soret effect on unsteady magnetohydrodynamic free convective flow past a semi-infinite vertical plate in the presence of viscous dissipation. The important correlation between viscosity and the Nusselt number discussed by Abu Nada et al. [35] also mentioned that viscosity plays a major role in their overall heat transfer behavior.

Despite the aforementioned literature has been reported, to the best of authors' knowledge there seems to be no attempts far been undertaken with regard to the numerical study of heat transfer enhancement in MHD free convection flow over vertical plate utilizing nanofluids. The novelty of the present study is to numerically investigate the effects of pertinent physical parameters on velocity and temperature distributions for two water based nanofluids. In this comprehensive numerical investigation we employed an extensively validated and robust finite element method owing to its advantages which includes it can be executed irrespective of the order or the degree of the governing differential equation. The weight function can be chosen from an independent set of functions other than the approximation function. The approximation function can be chosen from higher degree polynomial compared to the variational polynomial. In this paper formation of the problem and numerical procedure are presented in Sections 2 and 3. Sections 4 and 5 contain Grid independence study and validation of the code respectively. In Section 6 Results and Discussions of present study is reported. Finally summary of noteworthy results is presented in conclusion.

2. Mathematical formation of the problem

The Cartesian coordinate system $(\bar{x}, \bar{y}, \bar{z})$ and mathematical modeling of the problem under consideration are shown in Fig. 1. An unsteady free convective flow is chosen along the semi-infinite oscillatory plate embedded in a nanofluid. It is assumed that the plate oscillates with constant frequency in time $\bar{t}$. Flow direction is along the vertical porous plate which is the direction of $\bar{x}$-axis and is perpendicular to $\bar{z}$-axis. It is also assumed that the entire system is in rigid body rotation about $\bar{z}$-axis with constant velocity Ω. Initially at time $\bar{t} \leqslant 0$ plate and fluid are at rest and maintain at uniform temperature $\overline{T}_\infty$. At $\bar{t} > 0$ the plate has an oscillatory movement with time dependent velocity $\bar{u} = U_0(1 + \varepsilon \cos n\bar{t})$, where ε is small constant parameter and U_0 is the characteristic velocity. Along $\bar{z}$-axis an external magnetic field B_0 is acting which is greater than the induced magnetic field. No electric field is applied on plate so that oscillating plate can have small Reynolds number. The electrically nonconducting plate produces J_z to be constant due to current density conservation equation $\nabla \cdot J = 0$. It is further assumed that surface temperature $\overline{T}_w$ relatively more than the ambient temperature $\overline{T}_\infty$ and all physical quantities depends on variables $\bar{z}$ and $\bar{t}$. The governing boundary layer equations (Satya Narayana et al. [36]) under the Boussinesq approximations are as follows:

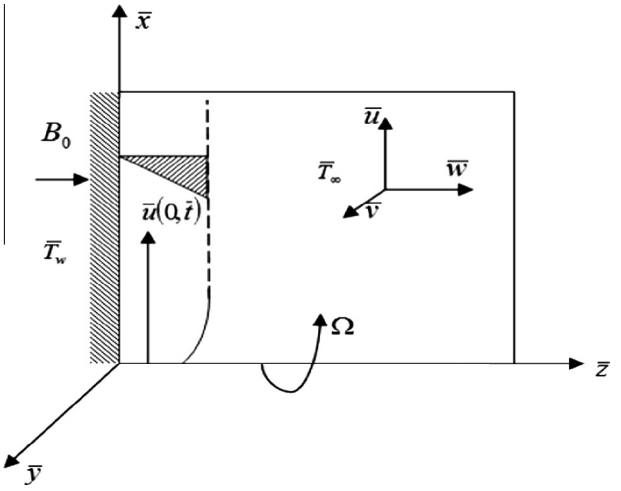

Figure 1 Physical model and Coordinate System of the problem.

$$\frac{\partial \bar{w}}{\partial \bar{z}} = 0 \tag{1}$$

$$\frac{\partial \bar{u}}{\partial \bar{t}} + \bar{w}\frac{\partial \bar{u}}{\partial \bar{z}} - 2\Omega\bar{v} = \frac{1}{\rho_{nf}}\left\{\mu_{nf}\frac{\partial^2 \bar{u}}{\partial \bar{z}^2} + (\rho\beta)_{nf} g(\overline{T} - \overline{T}_\infty) - \sigma_{nf}B_O^2\bar{u} - \frac{v_f}{k}\bar{u}\right\} \tag{2}$$

$$\frac{\partial \bar{v}}{\partial \bar{t}} + \bar{w}\frac{\partial \bar{v}}{\partial \bar{z}} + 2\Omega\bar{u} = \frac{1}{\rho_{nf}}\left\{\mu_{nf}\frac{\partial^2 \bar{v}}{\partial \bar{z}^2} - \sigma_{nf}B_O^2\bar{v} - \frac{v_f}{k}\bar{v}\right\} \tag{3}$$

$$\frac{\partial \overline{T}}{\partial \bar{t}} + \bar{w}\frac{\partial \overline{T}}{\partial \bar{z}} = \alpha_{nf}\frac{\partial^2 \overline{T}}{\partial \bar{z}^2} - \frac{1}{(\rho C_P)_{nf}}\frac{\partial q_r}{\partial \bar{z}} - \frac{Q_H}{(\rho C_P)_{nf}}(\overline{T} - \overline{T}_\infty) + \frac{\mu_{nf}}{(\rho C_P)_{nf}}\left(\frac{\partial \bar{u}}{\partial \bar{z}}\right)^2 \tag{4}$$

And the associated initial and boundary conditions (Ishigaki [37] and Ganapathy [38]) on the vertical surface and in free stream can defined as follows:

Introducing following non-dimensional quantities

$$\left.\begin{aligned} &z = \frac{U_o\bar{z}}{v_f}, \quad u = \frac{\bar{u}}{U_o}, \quad v = \frac{\bar{v}}{U_o}, \quad t = \frac{U_o^2\bar{t}}{v_f}, \quad n = \frac{v_f\bar{n}}{U_o^2}, \\ &\bar{w} = -w_0, \quad \theta = \frac{\overline{T} - \overline{T}_\infty}{\overline{T}_w - \overline{T}_\infty}, \quad S = \frac{w_o}{U_o^2}, \quad K = \frac{\rho_f k U_o^2}{v_f^2} \\ &M = \frac{\sigma_{nf}B_o^2 v_f}{\rho_f U_o^2}, \quad R = \frac{2\Omega v_f}{U_o^2}, \quad \Pr = \frac{(\rho C_p)_f v_f}{K_f}, \quad F = \frac{4\sigma^*\overline{T}_\infty^3}{kk^*}, \\ &Q = \frac{Q_H v_f^2}{K_f U_0^2}, \; E_C = \frac{U_o^2}{(\rho C_p)_f(\overline{T}_w - \overline{T}_\infty)} \end{aligned}\right\} \tag{10}$$

Substituting nanofluid properties Eqs. (6), (9) and (10) in Eqs. (2)–(4) we get the following non-dimensional equations.

$$L_1L_3\frac{\partial u}{\partial t} - L_1L_3S\frac{\partial u}{\partial z} - \frac{\partial^2 u}{\partial z^2} - L_1L_4Rv - L_1L_4\theta + L_1\left(M + \frac{1}{K}\right)u = 0 \tag{11}$$

$$\left.\begin{aligned} &for\ \bar{t} \leqslant 0\ \{\forall\ \bar{z} \qquad \bar{u}(\bar{z},\bar{t}) = 0,\ \ \bar{v}(\bar{z},\bar{t}) = 0,\ \ \overline{T} = T_\infty \\ &for\ \bar{t} > 0\ \begin{cases} \bar{z} = 0 & \bar{u}(0,\bar{t}) = U_0\ \left[1 + \frac{\varepsilon}{2}(e^{\mathrm{int}} + e^{-\mathrm{int}})\right],\ \ \bar{v}(0,\bar{t}) = 0, \quad \overline{T}(0,\bar{t}) = \overline{T}_\infty \\ \bar{z} \to \infty & \bar{u}(\infty,\bar{t}) \to 0, \quad \bar{v}(\infty,\bar{t}) \to 0,\ \ \overline{T}(\infty,\bar{t}) \to \overline{T}_\infty \end{cases} \end{aligned}\right\} \tag{5}$$

$$\left.\begin{aligned} &\mu_{nf} = \frac{\mu_f}{(1-\phi)^{2.5}}, \quad \alpha_{nf} = \frac{K_{nf}}{(\rho C_p)_{nf}}, \quad \rho_{nf} = (1-\phi)\rho_f + \phi\rho_s,\ (\rho C_p)_{nf} = (1-\phi)\,(\rho C_p)_f + \phi(\rho C_p)_s \\ &(\rho\beta)_{nf} = (1-\phi)\,(\rho\beta)_f + \phi(\rho\beta)_s\ K_{nf} = K_f[\tfrac{K_s+2K_f-2\phi\ (K_f-K_s)}{K_s+2K_f+2\phi\ (K_f-K_s)}], \\ &\sigma_{nf} = \sigma_f[1 + \tfrac{3(\sigma-1)\phi}{(\sigma+2)-(\sigma-1)\phi}],\ \sigma = \tfrac{\sigma_s}{\sigma_f} \end{aligned}\right\} \tag{6}$$

The radiative heat term (Brewster [39]) by using the Roseland approximation is given by

$$q_r = \frac{-4\sigma^*}{3k^*}\frac{\partial \overline{T}^4}{\partial \bar{z}} \tag{7}$$

where k^* and σ^* are mean absorption coefficient and Stefan–Boltzmann constant respectively. It is assumed that the temperature difference within the flow is sufficiently small such that $\overline{T}^4$ may be expressed as a linear function of the temperature by expanding in a Taylor series about $\overline{T}_\infty$ and neglecting the higher order terms

Thus we have $\overline{T}^4 \cong 4\overline{T}_\infty^3\overline{T} - 3\overline{T}_\infty^4$ (8)

Hence, from Eq. (7), using Eq. (8), we have

$$\frac{\partial q_r}{\partial \bar{z}} = -\frac{16\sigma^*\overline{T}_\infty^3}{3k^*}\frac{\partial^2 \overline{T}}{\partial \bar{z}^2} \tag{9}$$

$$L_1L_3\frac{\partial v}{\partial t} - L_1L_3S\frac{\partial v}{\partial z} - \frac{\partial^2 v}{\partial z^2} + L_1L_3Ru + L_1\left(M + \frac{1}{K}\right)v = 0 \tag{12}$$

$$L_5\Pr\frac{\partial \theta}{\partial t} - L_5\Pr S\frac{\partial \theta}{\partial z} - L_2\frac{\partial^2 \theta}{\partial z^2} + \Pr Q\theta - \Pr Ec\left(\frac{\partial u}{\partial z}\right)^2 = 0 \tag{13}$$

where $L_1 = (1-\phi)^{2.5}$, $L_2 = \frac{k_{nf}}{k_f} + \frac{4F}{3}$, $L_3 = 1 - \phi + \phi(\rho_s/\rho_f)$, $L_4 = 1 - \phi + \phi\left(\frac{(\rho\beta)_s}{(\rho\beta)_f}\right)$

$$L_5 = 1 - \phi + \phi\left(\frac{(\rho Cp)_s}{(\rho Cp)_f}\right)$$

Subject to initial and boundary conditions in dimensionless form are as follows:

$$\left.\begin{aligned} &for\ t \leqslant 0\ \{\forall\ z \qquad u(z,t) = 0,\ \ v(z,t) = 0,\ \theta(z,t) = 0 \\ &for\ t > 0\ \begin{cases} at\ z = 0 & u(0,t) = \ 1 + \frac{\varepsilon}{2}(e^{\mathrm{int}} + e^{-\mathrm{int}}) \qquad v(0,t) = 0, \quad \theta(0,t) = 1 \\ as\ z \to \infty & u(\infty,t) \to 0, \quad v(\infty,t) \to 0,\ \theta(\infty,t) \to 0 \end{cases} \end{aligned}\right\} \tag{14}$$

The velocity characteristic U_0 is defined as $U_0 = \{g\beta_f(T_w - T_\infty)\nu_f\}^{1/3}$.

The Skin friction coefficient C_f, the Nusselt number Nu are defined respectively as follows:

$$C_f = \mu_{nf}\left(\frac{\partial u}{\partial z}\right)_{z=0} \text{ and } Nu = -K_{nf}\left(\frac{\partial \theta}{\partial z}\right)_{z=0}$$

3. Numerical solution by FEM

The transformed system of coupled, nonlinear and non-homogeneous dimensionless partial differential Eqs. (11)–(13) under the boundary conditions Eq. (14) is solved numerically for both momentum and energy equations by using the extensively-validated and robust method known as finite element method. This method has five fundamental steps which are discretization of the domain, derivation of element equations, assembly of element equations, imposition of boundary conditions and solution of the assembled equations. An excellent description of these steps was presented in the text book by Reddy [40]. We have considered the free stream boundary condition. The boundary conditions for z at ∞ are replaced by a sufficiently large value where the velocity and temperature profiles approach to zero. We ran the developed code for different step sizes and we found that the results for all the profiles approach to zero asymptotically. After many trials, for computational flexibility we imposed $z_{\max} = 2.5$ where $z_{\max} \to \infty$ i.e., external to the boundary and thermal boundary layers. The finite element model of the original equation is given by means of algebraic equations in the unknown parameters with the finite element approximations as follows.

3.1. Variational formulation

The variational formulation associated with Eqs. (11)–(13) over a typical two-node linear element (z_e, z_{e+1}) is given by

$$\int_{z_e}^{z_{e+1}} w_1\left[L_1L_3\left(\frac{\partial u}{\partial t}\right) - L_1L_3S\left(\frac{\partial u}{\partial z}\right) - \left(\frac{\partial^2 u}{\partial z^2}\right) - L_1L_3Rv - L_1L_4\theta + L_1\left[M + \frac{1}{K}\right]u\right]dz = 0 \tag{15}$$

$$\int_{z_e}^{z_{e+1}} w_2\left[L_1L_3\left(\frac{\partial v}{\partial t}\right) - L_1L_3S\left(\frac{\partial v}{\partial z}\right) - \left(\frac{\partial^2 v}{\partial z^2}\right) + L_1L_3Ru + L_1\left[M + \frac{1}{K}\right]v\right]dz = 0 \tag{16}$$

$$\int_{z_e}^{z_{e+1}} w_3\left[L_5\mathrm{Pr}\left(\frac{\partial \theta}{\partial t}\right) - L_5\mathrm{Pr}S\left(\frac{\partial \theta}{\partial z}\right) - L_2\left(\frac{\partial^2 \theta}{\partial z^2}\right) + \mathrm{Pr}Q\theta - \mathrm{Pr}E_C\left(\frac{\partial u}{\partial z}\right)^2\right]dz = 0 \tag{17}$$

where w_1, w_2, w_3 are arbitrary test functions and may be viewed as the variation in u, v and θ respectively. After reducing the order of integration and nonlinearity, the following system of equations is obtained.

$$\int_{z_e}^{z_{e+1}} \left[L_1L_3(w_1)\left(\frac{\partial u}{\partial t}\right) - L_1L_3S(w_1)\left(\frac{\partial u}{\partial z}\right) - \left(\frac{\partial w_1}{\partial z}\right)\left(\frac{\partial u}{\partial z}\right) - L_1L_3R(w_1)v - L_1L_4(w_1)\theta + L_1\left(M + \frac{1}{K}\right)(w_1)u\right]dz - \left[(w_1)\left(\frac{\partial u}{\partial z}\right)\right]_{z_e}^{z_{e+1}} = 0 \tag{18}$$

$$\int_{z_e}^{z_{e+1}} \left[L_1L_3(w_2)\left(\frac{\partial v}{\partial t}\right) - L_1L_3S(w_2)\left(\frac{\partial v}{\partial z}\right) - \left(\frac{\partial w_2}{\partial z}\right)\left(\frac{\partial v}{\partial z}\right) + L_1L_3R(w_2)u + L_1\left(M + \frac{1}{K}\right)(w_2)v\right]dz - \left[(w_2)\left(\frac{\partial v}{\partial z}\right)\right]_{z_e}^{z_{e+1}} = 0 \tag{19}$$

$$\int_{z_e}^{z_{e+1}} \left[L_5\mathrm{Pr}(w_3)\left(\frac{\partial \theta}{\partial t}\right) - L_5\mathrm{Pr}S(w_3)\left(\frac{\partial \theta}{\partial z}\right) - L_2\left(\frac{\partial w_3}{\partial z}\right)\left(\frac{\partial \theta}{\partial z}\right) + \mathrm{Pr}Q(w_3)\theta - \mathrm{Pr}E_C(w_3)\left(\frac{\partial \bar{u}}{\partial z}\right)\left(\frac{\partial u}{\partial z}\right)\right]dz - \left[(w_3)\left(\frac{\partial \theta}{\partial z}\right)\right]_{z_e}^{z_{e+1}} = 0 \tag{20}$$

3.2. Finite element formulation

The finite element model may be obtained from Eqs. (18)–(20) by substituting finite element approximations of the form:

$$u = \sum_{j=1}^{2} u_j^e\psi_j^e,\ v = \sum_{j=1}^{2} v_j^e\psi_j^e,\ \theta = \sum_{j=1}^{2} \theta_j^e\psi_j^e \tag{21}$$

With $w_1 = w_2 = w_3 = \psi_j^e (i = 1, 2)$, where u_j^e, v_j^e and θ_j^e are the velocity in the direction of x-axis, y-axis and temperature respectively at the j^{th} node of typical eth element (z_e, z_{e+1}) and ψ_i^e are the shape functions for this element (z_e, z_{e+1}) and are taken as follows:

$$\psi_1^e = \frac{z_{e+1} - z}{z_{e+1} - z_e} \text{ and } \psi_2^e = \frac{z - z_e}{z_{e+1} - z_e},\ z_e \leqslant z \leqslant z_{e+1} \tag{22}$$

By choosing these functions into Eqs. (18)–(20) yields local stiffness matrices. These are $\{[K^{mn}], [M^{mn}]\}$ and $\{\{u^e\}, \{v^e\}, \{\theta^e\}, \{u'^e\}, \{v'^e\}, \{\theta'^e\}$ and $\{b^{me}\}\}(m, n = 1, 2, 3)$ are the set of matrices of order 2×2 and 2×1 respectively, such stiffness matrices in terms of local nodes in each element are assembled using inter element continuity and equilibrium conditions to obtain the global matrices and the *prime* ($'$) indicates $\frac{d}{dz}$.

Therefore, the finite element model of the equations for eth element thus formed is given by

$$\begin{bmatrix} [K^{11}] & [K^{12}] & [K^{13}] \\ [K^{21}] & [K^{22}] & [K^{23}] \\ [K^{31}] & [K^{32}] & [K^{33}] \end{bmatrix} \begin{bmatrix} \{u^e\} \\ \{v^e\} \\ \{\theta^e\} \end{bmatrix} + \begin{bmatrix} [M^{11}] & [M^{12}] & [M^{13}] \\ [M^{21}] & [M^{22}] & [M^{23}] \\ [M^{31}] & [M^{32}] & [M^{33}] \end{bmatrix} \begin{bmatrix} \{u'^e\} \\ \{v'^e\} \\ \{\theta'^e\} \end{bmatrix} = \begin{bmatrix} \{b^{1e}\} \\ \{b^{2e}\} \\ \{b^{3e}\} \end{bmatrix} \tag{23}$$

These matrices are defined as follows:

$$\begin{cases} K_{ij}^{11} = -L_1 L_3 S \int_{z_e}^{z_{e+1}} \left[(\psi_i^e) \left(\frac{\partial \psi_j^e}{\partial z} \right) \right] dz + \int_{z_e}^{z_{e+1}} \left[\left(\frac{\partial \psi_i^e}{\partial z} \right) \left(\frac{\partial \psi_j^e}{\partial z} \right) \right] dz \\ + L_1 \left(M + \frac{1}{K} \right) \int_{z_e}^{z_{e+1}} [(\psi_i^e)(\psi_j^e)] dz, \\ K_{ij}^{12} = -L_1 L_3 R \int_{z_e}^{z_{e+1}} (\psi_i^e)(\psi_j^e) dz, \\ K_{ij}^{13} = -L_1 L_4 \int_{z_e}^{z_{e+1}} (\psi_i^e)(\psi_j^e) dz, M_{ij}^{11} = L_1 L_3 \int_{z_e}^{z_{e+1}} (\psi_i^e)(\psi_j^e) dz, \\ M_{ij}^{12} = M_{ij}^{13} = 0, \end{cases}$$

$$\begin{cases} K_{ij}^{22} = -L_1 L_3 S \int_{z_e}^{z_{e+1}} \left[(\psi_i^e) \left(\frac{\partial \psi_j^e}{\partial z} \right) \right] dz + \int_{z_e}^{z_{e+1}} \left[\left(\frac{\partial \psi_i^e}{\partial z} \right) \left(\frac{\partial \psi_j^e}{\partial z} \right) \right] dz \\ + L_1 \left(M + \frac{1}{K} \right) \int_{z_e}^{z_{e+1}} [(\psi_i^e)(\psi_j^e)] dz, \\ K_{ij}^{21} = L_1 L_3 R \int_{z_e}^{z_{e+1}} (\psi_i^e)(\psi_j^e) dz, K_{ij}^{23} = 0, \\ M_{ij}^{22} = L_1 L_3 \int_{z_e}^{z_{e+1}} (\psi_i^e)(\psi_j^e) dz, \\ M_{ij}^{21} = M_{ij}^{23} = 0, \end{cases}$$

$$\begin{cases} K_{ij}^{31} = -\mathrm{Pr}(Ec) \int_{z_e}^{z_{e+1}} (\psi_i^e) \left(\frac{\partial \bar{u}}{\partial z} \right) \left(\frac{\partial \psi_j^e}{\partial z} \right) dz, \\ K_{ij}^{32} = 0, K_{ij}^{33} = -L_5 \mathrm{Pr} S \int_{z_e}^{z_{e+1}} \left[(\psi_i^e) \left(\frac{\partial \psi_j^e}{\partial z} \right) \right] dz \\ - L_2 \int_{z_e}^{z_{e+1}} \left[\left(\frac{\partial \psi_i^e}{\partial z} \right) \left(\frac{\partial \psi_j^e}{\partial z} \right) \right] dz + \mathrm{Pr} Q \int_{z_e}^{z_{e+1}} (\psi_i^e)(\psi_j^e) dz \\ M_{ij}^{31} = 0, M_{ij}^{32} = 0, M_{ij}^{33} = L_5 \mathrm{Pr} \int_{z_e}^{z_{e+1}} (\psi_i^e)(\psi_j^e) dz \end{cases}$$

$$\begin{cases} b_i^{1e} = \left[(\psi_i^e) \left(\frac{\partial u}{\partial z} \right) \right]_{z_e}^{z_{e+1}}, \; b_i^{2e} = \left[(\psi_i^e) \left(\frac{\partial v}{\partial z} \right) \right]_{z_e}^{z_{e+1}}, \\ b_i^{3e} = \left[(\psi_i^e) \left(\frac{\partial \phi}{\partial z} \right) \right]_{z_e}^{z_{e+1}} \end{cases}$$

4. Grid independence study

The grid independence is conducted by dividing the entire domain into successively sized grids $81 \times 81, 101 \times 101$ and 121×121. For all the computations 101 intervals of equal length 0.01 are considered. At each node three functions are to be evaluated so that, after assembly of elements a set of 303 nonlinear equations is formed, consequently an iterative scheme is adopted and by introducing boundary conditions system of equations is solved. The solution is assumed to be converged when the difference satisfies the desired accuracy 10^{-7}. An excellent convergence for all the results is achieved.

5. Validation of the code

The correctness of this numerical scheme and MATLAB code is ensured by comparing the present results for skin friction coefficient and Nusselt number with the results obtained through analytical approach whenever $Ec = 0$. It confirms that present results are in excellent agreement with the results reported by Satya Narayana et al. [36] which are shown in Table 1. Therefore, the developed code can be used with a great confidence in the numerical results presented subsequently to study the problem considered in this paper.

6. Results and discussion

The primary interest of this paper is the numerical study of heat transfer enhancement in free convection flow over vertical plate with viscous dissipation and radiation utilizing nanofluids. Additionally the influence of K, M, R, S, ϕ, Q *and* Pr on the nanofluid velocity and temperature as well as the skin friction and Nusselt number distribution for *Cu-water* and *Al_2O_3-water* nanofluids is discussed, and is represented graphically in Figs. 2–16. In this paper the values that are chosen as constants are $n = 10, nt = \pi/2, \varepsilon = 0.02$. And other parameters $K, M, R, S, \phi, Q, Ec, F$ *and* Pr are changes over a range, which are mentioned in the legends of figures. Furthermore Table 2 shows thermo-physical properties of (H_2O, Cu, Al_2O_3 and TiO_2).

The behavior of Skin-friction and Nusselt number for different values of M, ϕ *and* Ec when Pr = 6.2 are presented in Table 3. It is evident from the table that skin friction coefficient decreases with the increase of M while the skin friction coefficient increases with an increase of ϕ *and* Ec. Physically this means that velocity at the wall decreases due

Table 1 Comparison of Skin friction and Nusselt number for various values of Pr when $Ec = 0$.

Pr	Previous results Satya Narayana et al. [36]		Present results	
	C_f	Nu	C_f	Nu
0.5	2.3159708	5.9674	2.3159709	5.9674101
1.0	2.2567503	6.0461	2.2567504	6.0461012
1.5	2.1972895	6.1259	2.1972896	6.1259001
2.0	2.1376083	6.2066	2.1376084	6.2066013

Table 2 Thermo-physical properties of water and nanoparticles.

Physical properties	H_2O	Cu	Al_2O_3	TiO_2
Cu (j/kg k)	4179	385	765	686.2
ρ (kg/m^3)	997.1	8933	3970	4250
K (W/m k)	0.613	400	40	8.9538
$\beta \times 10^{-5}$ (1/k)	21	1.67	0.85	0.9

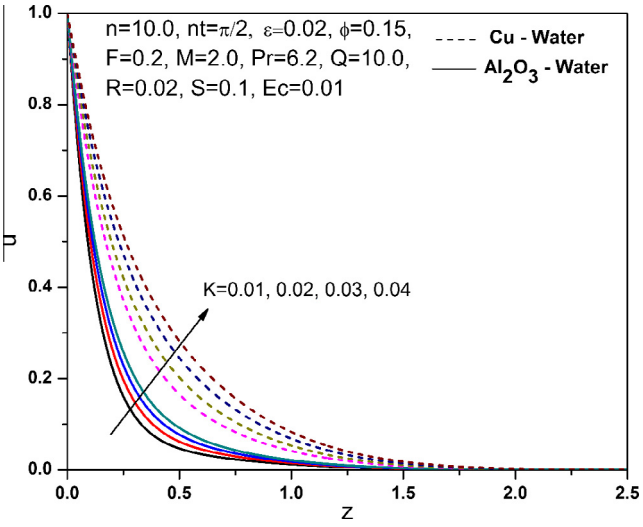

Figure 2 Velocity Profiles for K.

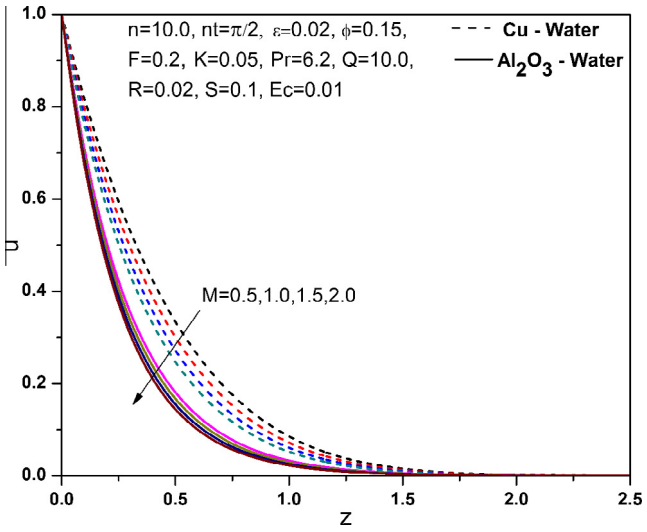

Figure 3 Velocity Profiles for M.

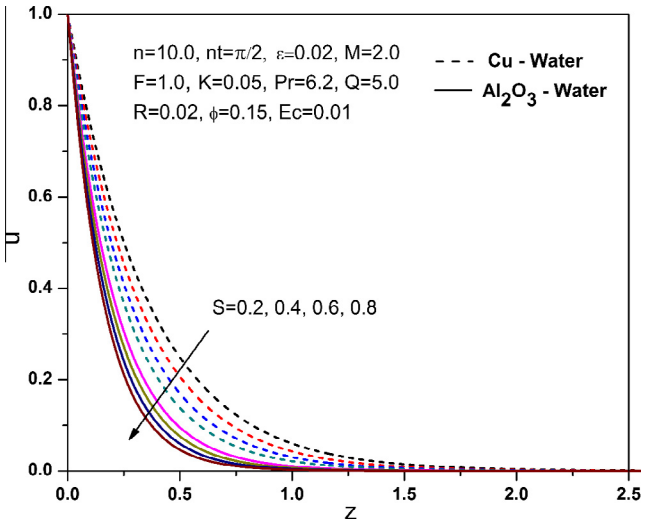

Figure 5 Velocity Profiles for S.

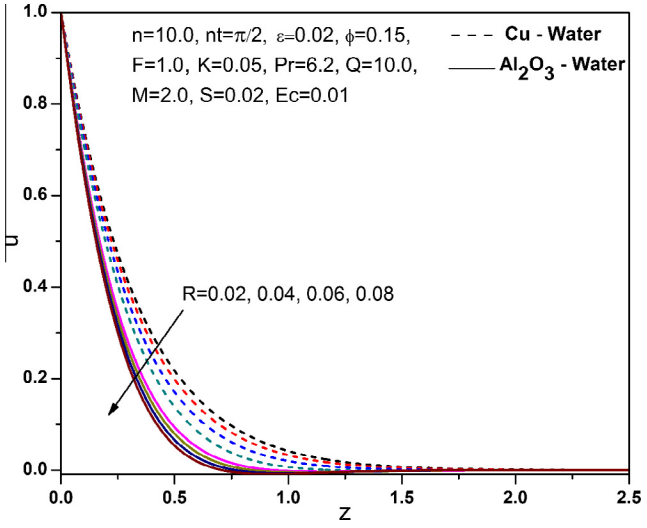

Figure 4 Velocity Profiles for R.

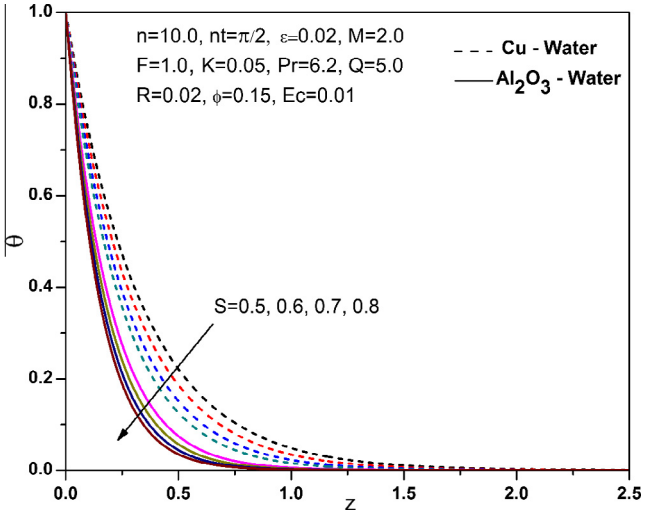

Figure 6 Temperature Profiles for S.

to the reduction in skin friction. Further it is observed that Nusselt number is found to reduce with an increase of *M and* ϕ while the Nusselt number is enhanced with the increase of *Ec*. Physically this means that heat transfer rate at the surface is decreased due to reduction in Nusselt number.

It interesting to note that an increase in the permeability parameter *K* of the porous medium leads to decrease in the thickness of thermal boundary layer owing to that the presence of porous medium enhances the resistance to the flow resulting in reduction in fluid. This physical behavior is illustrated in Fig. 2. Therefore, porous medium impact is significant on the reduction in boundary layer. An application of magnetic field normal to the fluid flow produces resistive type force which is also called as Lorentz force, and it acts against the relative motion of the fluid. Therefore, this force slows down the motion of the fluid in the boundary layer. This physical behavior is characterized by velocity profiles in the immediate vicinity of boundary layer as shown in Fig. 3. An increase in magnetic field *M* along the surface causes to decrease the velocity of nanofluid. Velocity profiles for different values of rotational parameter *R* are presented in Fig. 4, in which nanofluid velocity profiles decrease with the increase in rotational parameter due to the reason that the magnitude of the rotational drag force is reduced. Here it is to be pointed that coriolis body forces arise in momentum equations via $-Rv$ *and* Ru respectively.

The influence of suction on velocity and temperature profiles is shown in Figs. 5 and 6 respectively. The velocity and temperature profiles start with the plate velocity and decreased to zero asymptotically with corresponding boundary conditions. Furthermore, the nanofluid velocity and temperature profiles decrease with the increase in the suction parameter *S* and this is due to the fact that the suction brought the fluid near the wall surface; consequently, it stabilizes the both boundary and thermal boundary layer growths, and this observation agrees with the physical point of view.

Whenever the volume fraction ϕ of nanoparticles increases, the thermal conductivity of fluid and thickness of thermal boundary layer increase, and this physical behavior is exemplified in Figs. 7 and 8. Here in these graphs the velocity profiles

Please cite this article in press as: Sheri SR, Thumma T, Numerical study of heat transfer enhancement in MHD free convection flow over vertical plate utilizing nanofluids, Ain Shams Eng J (2016), http://dx.doi.org/10.1016/j.asej.2016.06.015

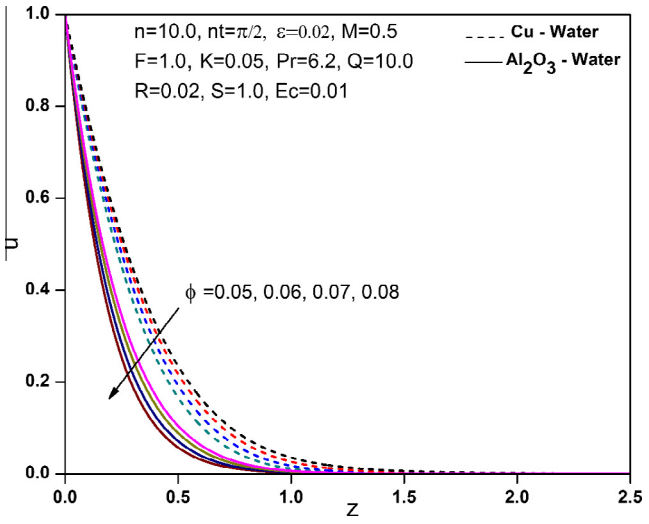

Figure 7 Velocity Profiles for ϕ.

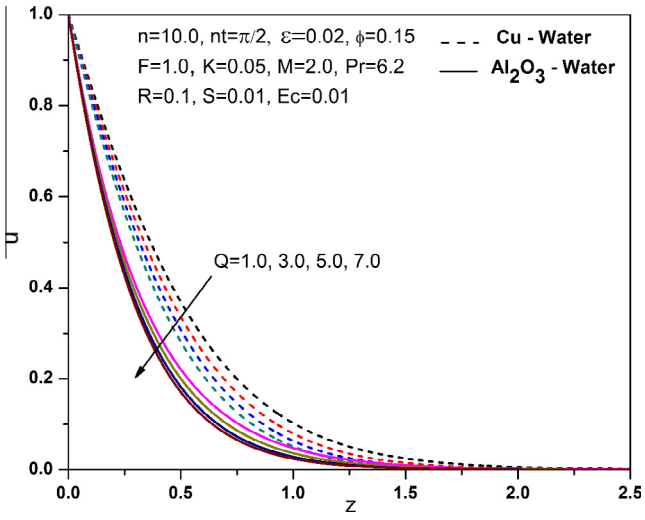

Figure 9 Velocity Profiles for Q.

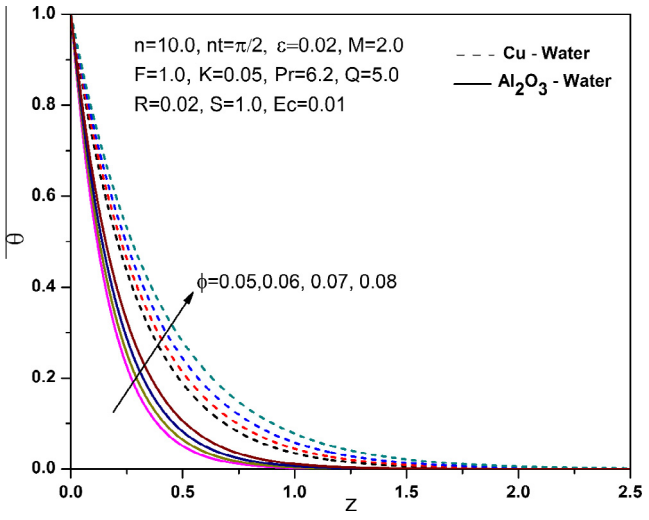

Figure 8 Temperature Profiles for ϕ.

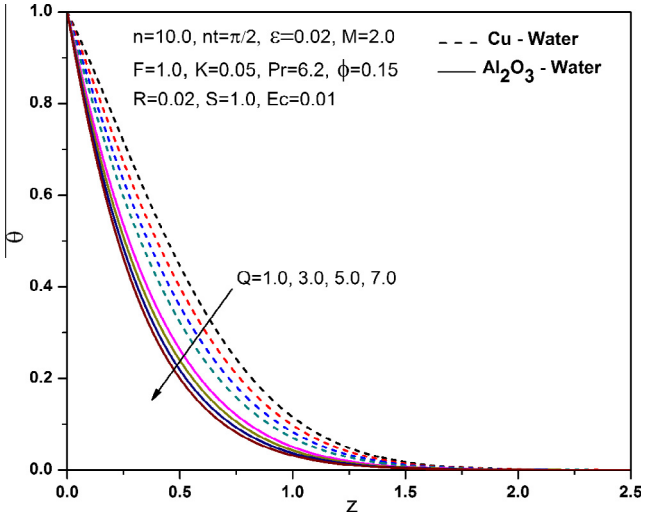

Figure 10 Temperature Profiles for Q.

are decreased and temperature distribution profiles are increased with the increase in volume fraction parameter of nanofluid respectively. However, the thermal conductivity of water based nanofluids increases as the nanoparticle size increases because the low viscosity of the base fluid promotes the clustering of nanoparticles and this particle clustering forms interconnecting channels for thermal energy to propagate. So as volume fraction increases the thermal conductivity of water based nanofluid is enhanced. Furthermore graphs are exhibiting that the velocity profiles for Al_2O_3-*water* nanofluid are relatively lesser than those of Cu-*water* nanofluid due to decrease in thickness of the boundary layer, while the temperature distribution in the *Cu-water* nanofluid is greater than Al_2O_3-*water* nanofluid, since by the reason of the fact that copper has significantly high conductivity than the alumina and therefore, the thickness of thermal boundary layer of Cu-*water* nanofluid is greater than the Al_2O_3-*water* nanofluid.

The nanofluid velocity and temperature profiles for different values of heat source parameter Q are represented in Figs. 9 and 10. These graphs illustrate that an increase of Q decreases

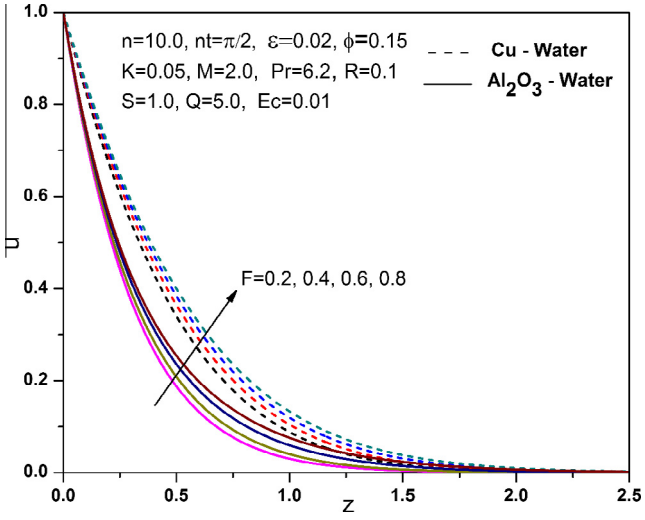

Figure 11 Velocity Profiles for F.

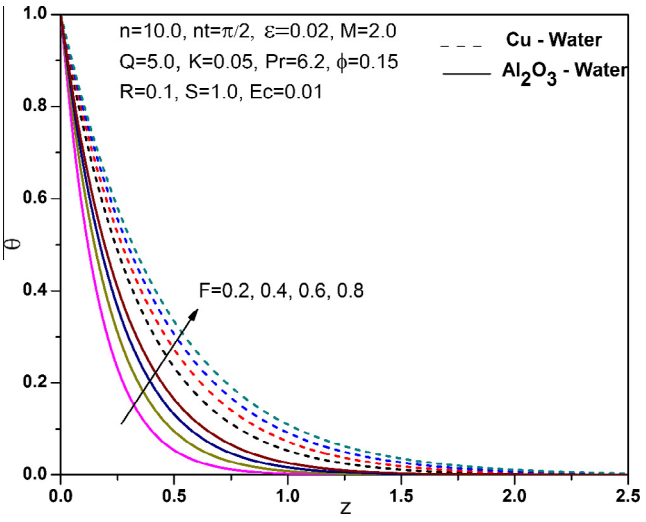

Figure 12 Temperature Profiles for F.

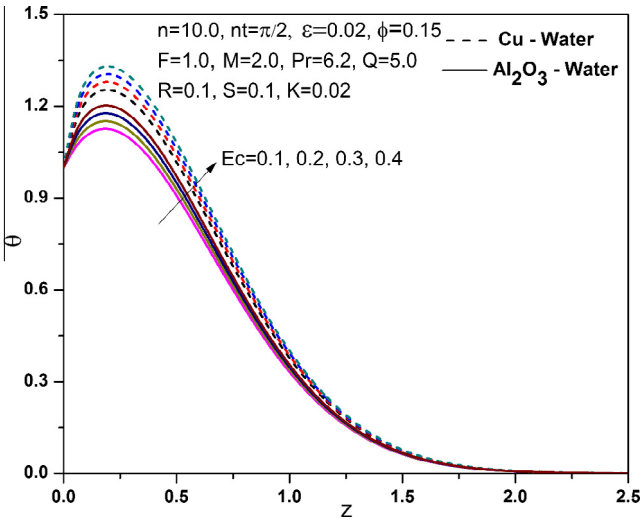

Figure 14 Temperature Profiles for Ec.

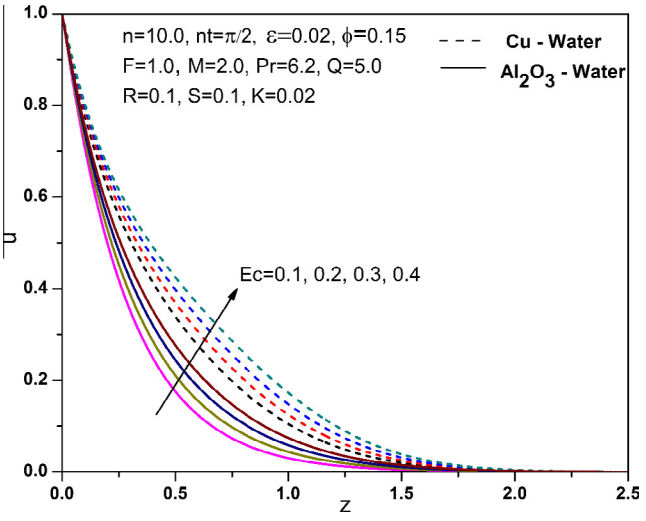

Figure 13 Velocity Profiles for Ec.

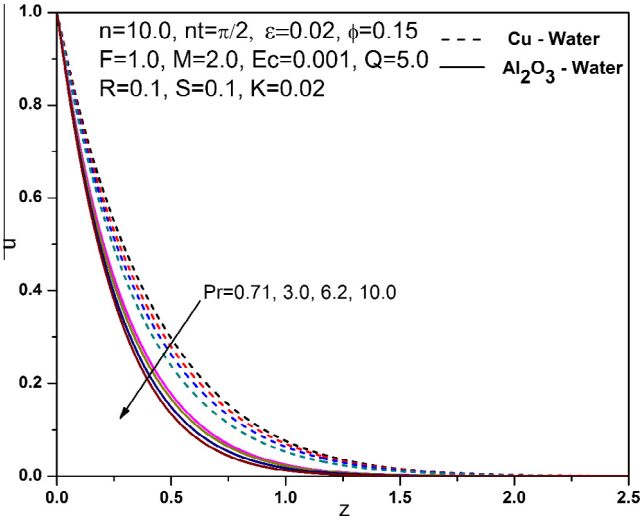

Figure 15 Velocity Profiles for Pr.

velocity and temperature profiles at the boundary and thermal boundary layers of nanofluids respectively, owing to the absorption of energy in the boundary layers. Therefore when heat is absorbed the buoyancy force decreased which then resists the flow rate. Furthermore for various values of thermal radiation F, the velocity and temperature of profiles of water based nanofluids (Cu-*water* and Al_2O_3-*water*) are shown in Figs. 11 and 12. It is evident from the figures that with the increase in thermal radiation parameter values caused to enhance the hydrothermal boundary layers. The presence of thermal radiation is very significant on the variation of temperature. It seems that temperature increases rapidly in the presence of thermal radiation throughout the boundary layer. It may be attributed to the fact that absorbed Roseland radiative parameter diminishes the corresponding heat flux and hence raising in the rate of radiative heat transfer to the fluid causing the raise in temperature of the fluid and increase in the thickness of boundary and thermal boundary layers.

The correlation between the kinetic energy in the flow and the enthalpy refers to an Eckert number (Schlichting boundary layer theory). Due to internal friction heating between molecules of the fluid, the amount of mechanical energy changed to thermal energy and this thermal energy is reserved in the fluid. Therefore an increase in Eckert number Ec causes an increase in thermal energy contributing to the flow and will enhance the temperature of the water based nanofluids throughout the thermal boundary layer in the porous medium. It is also observed that an increase in viscous dissipation parameter increases the velocity of nanofluids owing to energy release which increases the momentum. Thus by the decrease in density of the nanofluid in the boundary layer due to heat generated by viscous flow, which in turn causes the thickness of the boundary layer to be enhanced. This physical behavior is depicted in Figs. 13 and 14.

The variations in the velocity and temperature profiles for different values of Prandtl number Pr are depicted in Figs. 15 and 16. Prandtl number refers to the relative contribution of momentum diffusion to thermal diffusion in the boundary layer regime. With the increase in Prandtl number leads to a

Please cite this article in press as: Sheri SR, Thumma T, Numerical study of heat transfer enhancement in MHD free convection flow over vertical plate utilizing nanofluids, Ain Shams Eng J (2016), http://dx.doi.org/10.1016/j.asej.2016.06.015

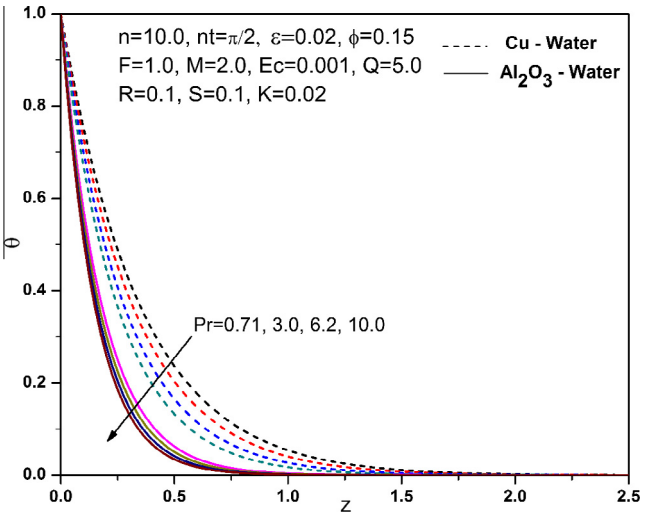

Figure 16 Temperature Profiles for Pr.

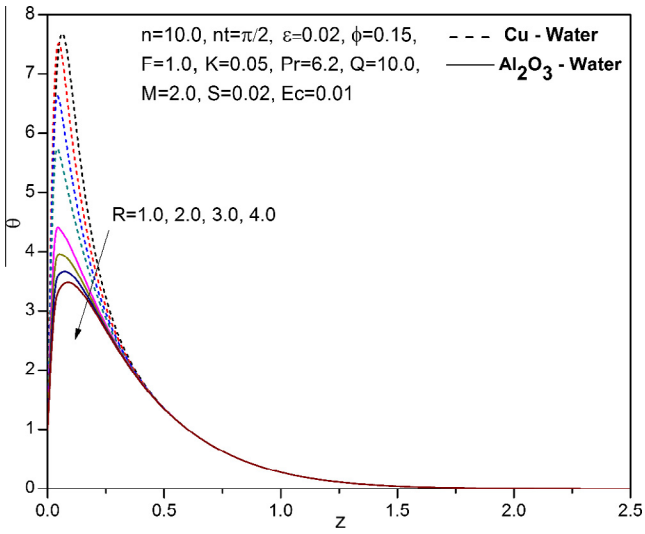

Figure 17 Temperature Profiles for R.

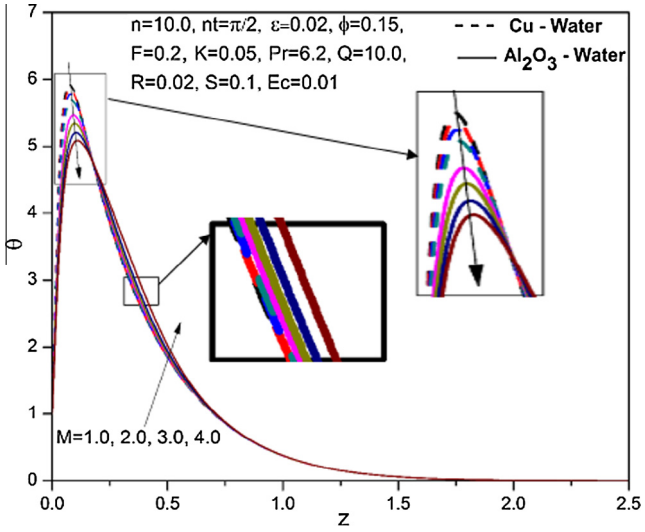

Figure 18 Temperature Profiles for M.

decrease in the velocity at the wall which then approaches the free stream value, and this is due to the reason that momentum diffusion rate exceeds thermal diffusion rate. Furthermore an increase in the Prandtl number results in a decrease in the temperature distribution in the boundary layer. The physical reason is that smaller values of Pr are equivalent to an increasing thermal conductivity, and therefore heat is able to diffuse away from the heated surface more rapidly than at higher values of Pr. Hence the boundary layer becomes thicker and the rate of heat transfer is reduced. Therefore an increase in Pr cause to reduction in thickness of the thermal boundary layer.

The effect of rotation parameter R and magnetic field parameter M on temperature distribution of two water based nanofluids is represented in Figs. 17 and 18 respectively. It is evident from Fig. 17 that the temperature profiles are decreased with an increase in rotational parameter. This implies that the rotation retards the temperature throughout the boundary layer region. Here, temperature profiles start with the temperature of the plate at the surface and then increase with a distance from the surface, reach to maximum value in the vicinity of the plate and thereafter, decrease monotonically to zero at the free stream. This is due to reason the reduction in the coriolis body force. We infer from Fig. 18 that temperature profiles are decreased near surface of the plate and increased in the region away from the plate with an increase in magnetic field parameter. Furthermore, it is worth mentioning here that the fluid temperature profiles start with the temperature of the plate at the surface and then it attains a maximum value and decays rapidly near the surface of the

Table 3 Values of Skin friction and Nusselt number for various values of M, ϕ, Ec and R.

				C_f			Nu		
M	ϕ	Ec	R	Cu	Al_2O_3	TiO_2	Cu	Al_2O_3	TiO_2
0.0	0.1	0.001	0.02	0.8561	0.8471	0.7961	0.2357	0.2278	0.2192
0.5	0.1	0.001	0.02	0.8497	0.8407	0.7897	0.2342	0.2263	0.2177
1.0	0.1	0.001	0.02	0.8433	0.8343	0.7833	0.2327	0.2248	0.2162
0.0	0.2	0.001	0.02	0.8625	0.8535	0.8025	0.2312	0.2233	0.2147
0.0	0.3	0.001	0.02	0.8689	0.8599	0.8089	0.2381	0.2302	0.2216
0.0	0.1	0.002	0.02	0.8769	0.8679	0.8259	0.2432	0.2347	0.2261
0.0	0.1	0.003	0.02	0.8977	0.8887	0.8377	0.2507	0.2416	0.233
0.0	0.1	0.001	0.04	0.9041	0.9032	0.8981	0.2271	0.2193	0.2104
0.0	0.1	0.001	0.06	0.9105	0.9096	0.9032	0.2271	0.2193	0.2104

Please cite this article in press as: Sheri SR, Thumma T, Numerical study of heat transfer enhancement in MHD free convection flow over vertical plate utilizing nanofluids, Ain Shams Eng J (2016), http://dx.doi.org/10.1016/j.asej.2016.06.015

boundary layer; thereafter, temperature decreases monotonically to asymptotic value according to the boundary condition. Thus the presence of magnetic field decreases the momentum boundary layer thickness and enhances the thickness of the thermal boundary layer.

7. Conclusions

The numerical study of heat transfer enhancement in free convection flow over vertical plate with viscous dissipation and radiation utilizing nanofluids has been investigated in detail. The effects of governing parameters, such as $K, M, R, S, \phi, Q, F, Ec$ *and* Pr are studied and are exemplified with the aid of graphs. Significant findings from the study are, an increase in K, F *and* Ec tends to enhance the velocity of the nanofluid while the other parameters M, R, S, ϕ, Q *and* Pr tend to decelerate the velocity of the nanofluid. Furthermore F, ϕ, M *and* Ec tend to accelerate the temperature profiles while the S, Q, R *and* Pr have reverse effect on it. An increase in M tends to reduce the Skin friction while the increase of R, ϕ *and* Ec tends to increase the Skin friction. Finally an increase in M tends to reduce the Nusselt number while the increase of Ec *and* ϕ tends to enhance the Nusselt number but Nusselt number remains unchanged for R. Finally it is noticed from the graphs that velocity and temperature profiles for Al_2O_3 - *water* are comparatively less than those of *Cu* - *water* nanofluid.

Acknowledgment

One of the authors (Siva Reddy Sheri) acknowledges financial support of University Grants Commission, New Delhi, under Major Research Project F. No. 42-22/2013(SR).

References

[1] Choi S. Enhancing thermal conductivity of fluids with Nanoparticles. In: Siginer DA, Wang HP, editors. In developments and Applications of non-Newtonian flows, vol. 66. ASME; 1995. p. 99–105.
[2] Choi SUS, Zhang ZG, Yu W, Lockwood FE, Grulke EA. Anomalously thermal conductivity enhancement in nanotube suspensions. Appl Phys Lett 2001;79:2252.
[3] Hatami M, Domairry G. Transient vertically motion of a soluble particle in a Newtonian fluid media. Powder Technol 2014;253:481–5.
[4] Ahmadi AR, Zahmatkesh A, Hatami M, Ganji DD. A comprehensive analysis of the flow and heat transfer for a nanofluid over an unsteady stretching flat plate. Powder Technol 2014;258:125–33.
[5] Hatami M, Ganji DD. Motion of a spherical particle on a rotating parabola using Lagrangian and high accuracy Multi-step Differential Transformation Method. Powder Technol 2014;258:94–8.
[6] Rahimi-Gorji M, Pourmehran O, Hatami M, Ganji DD. Statistical optimization of microchannel heat sink (MCHS) geometry cooled by different nanofluids using RSM analysis. Eur Phys J Plus 2015;130(2):1–21.
[7] Ghasemi SE, Hatami M, Sarokolaie AK, Ganji DD. Study on blood flow containing nanoparticles through porous arteries in presence of magnetic field using analytical methods. Physica E 2015;70:146–56.
[8] Sheikholeslami M, Ganji DD. Nanofluid flow and heat transfer between parallel plates considering Brownian motion using DTM. Comput Methods Appl Mech Eng 2015;283:651–63.
[9] Buongiorno J. Convective transport in Nanofluids. ASME J Heat Transfer 2006;128:240–50.
[10] Tiwari RK, Das MK. Heat transfer augmentation in a two-sided lid-driven differentially heated square cavity utilizing Nanofluids. Int J Heat Mass Transfer 2007;50:2002–18.
[11] Hatami M, Ganji DD. Natural convection of sodium alginate (SA) non-Newtonian nanofluid flow between two vertical flat plates by analytical and numerical methods. Case Stud Thermal Eng 2014;2:14–22.
[12] Sheikholeslami M, Ellahi R. Three dimensional mesoscopic simulation of magnetic field effect on natural convection of nanofluid. Int J Heat Mass Transf 2015;89:799–808.
[13] Chamkha AJ, Gorla RSR, Ghodeswar K. Non-similar solution for natural convective boundary layer flow over a sphere embedded in a porous medium saturated with a nanofluid. Transp Porous Media 2011;86:13–22.
[14] Sheikholeslami M, Ashorynejad HR, Rana P. Lattice Boltzmann simulation of nanofluid heat transfer enhancement and entropy generation. J Mol Liq 2016;214:86–95.
[15] Nield D, Bejan A. Convection in porous media. 4th ed. New York: Springer; 2013.
[16] Sheikholeslami M, Vajravelu K, Rashidi MM. Forced convection heat transfer in a semi annulus under the influence of a variable magnetic field. Int J Heat Mass Transf 2016;92:339–48.
[17] Chamkha J, Aly AM. MHD free convection flow of a nanofluid past a vertical plate in the presence of Heat Generation or Absorption effects. Chem Eng Comm 2011;198:425–41.
[18] Sheikholeslami M, Gorji-Bandpy M, Ganji DD, Rana P, Soheil S. Magnetohydrodynamic free convection of Al_2O_3-water nanofluid considering Thermophoresis and Brownian motion effects. Comput Fluids 2014;94:147–60.
[19] Ghasemi SE, Hatami M, Mehdizadeh Ahangar GHR, Ganji DD. Electrohydrodynamic flow analysis in a circular cylindrical conduit using Least Square Method. J Electrostat 2014;72(1):47–52.
[20] Sheikholeslami M. Effect of spatially variable magnetic field on ferrofluid flow and heat transfer considering constant heat flux boundary condition. Eur Phys J Plus 2014;129(11).
[21] Ellahi R. The effects of MHD and temperature dependent viscosity on the flow of non-Newtonian nanofluid in a pipe: analytical solutions. Appl Math Model 2013;37(3):1451–67.
[22] Sheikholeslami M, Soleimani Soheil, Ganji DD. Effect of electric field on hydrothermal behavior of nanofluid in a complex geometry. J Mol Liq 2016;213:153–61.
[23] Hamad MAA, Pop I. Unsteady MHD free convection flow past a vertical permeable flat plate in a rotating frame of reference with constant heat source in a Nanofluid. Heat Mass Transfer 2011;47:1517–24.
[24] Sheikholeslami M, Rashidi MM, Ganji DD. Effect of non-uniform magnetic field on forced convection heat transfer of Fe_3O_4–water nanofluid. Comput Methods Appl Mech Eng 2015;294:299–312.
[25] Sheikholeslami M, Rashidi MM, Ganji DD. Numerical investigation of magnetic nanofluid forced convective heat transfer in existence of variable magnetic field using two phase model. J Mol Liq 2015;212:117–26.
[26] Sheikholeslami M, Ganji DD. Hydrothermal analysis in engineering using control volume finite element method. 1st ed. Elsevier-Academic Press; 2015.
[27] Sheikholeslami M, Hayat T, Alsaedi A. MHD free convection of Al_2O_3–water nanofluid considering thermal radiation: a numerical study. Int J Heat Mass Transf 2016;96:513–24.

[28] Arpaci VS. Effect of thermal radiation on the laminar free convection from a heated vertical plate. Int J Heat Mass Transfer 1968;11:871–81.
[29] Chamkha AJ, Abbasbandy S, Rashad AM, Vajravelu K. Radiation effects on mixed convection over a wedge embedded in a porous medium filled with a Nanofluid. Transp Porous Med 2012;91:261–79.
[30] Olanrewaju PO, Olanrewaju MA, Adesanya AO. Boundary layer flow of Nanofluids over a moving surface in a flowing fluid in the presence of radiation. Int J Appl Sci Tech 2012;2(1):274.
[31] Arefmanesh A, Mahmoodi M. Effects of uncertainties of viscosity models for Al_2O_3-water nanofluid on mixed convection numerical simulations. Int J Therm Sci 2011;50:1706.
[32] Sheikholeslami M, Ganji DD, Javed MY, Ellahi R. Effect of thermal radiation on magnetohydrodynamics nanofluid flow and heat transfer by means of two phase model. J Magn Magn Mater 2015;374:36–43.
[33] Domairry G, Hatami M. Squeezing Cu–water nanofluid flow analysis between parallel plates by DTM-Pade Method. J Mol Liq 2014;193:37–44.
[34] Siva Reddy S, Srinivasan R. Soret effect on unsteady magneto-hydrodynamic free convective flow past a semi–infinite vertical plate in the presence of viscous dissipation. Int J Comput Methods Eng Sci Mech 2015;16:132–41.
[35] Abu Nada E, Masoud Z, Oztop HF, Campo A. Effect of nanofluid variable properties on natural convection in enclosures. Int J Therm Sci 2010;49(3):479.
[36] Satya Narayana PV, Venkateswarlu B, Venkataramana S. Thermal radiation and heat source effects on a MHD nanofluid past a vertical plate in a rotating system with porous medium. Heat Transfer Asian Res 2015;44(1):1–19.
[37] Ishigaki H. Periodic boundary layer near a two-dimensional stagnation point. J Fluid Mech 1970;43:477–86.
[38] Ganapathy R. A note on oscillatory Couette flow in a rotating system. ASME J Appl Mech 1994;61:208–19.
[39] Brewster MQ. Thermal radiative transfer properties. Wiley; 1972.
[40] Reddy JN. An introduction to the finite element method. New York: McGraw-Hill Book Company; 2006.

Dr Siva Reddy Sheri is an Assistant Professor in the Department of Engineering Mathematics, GITAM University, Hyderabad Campus, Hyderabad, Telangana, India. He received his Ph.D. in the Mathematics from Osmania University, Hyderabad, India. He has more than thirteen years of experience of teaching and research. His current area of research study includes Fluid dynamics, Magnetohydrodynamics and Heat and Mass transfer. He got Major Research Project from University Grants Commission (UGC) [F.No:42-22/2013 (SR) letter dated 12-03-2013]. He has published more than forty research papers in national/International journals of repute. He has received Best Researcher Award-2015 at 6th Convocation (GITAM University) held in Hyderabad in recognition of extensive research work in Mathematics.

Thirupathi Thumma is working as an Assistant Professor of Mathematics in the Department of Mathematics, B V Raju Institute of Technology, Medak. He did M.Sc. Mathematics from Kakatiya University, Warangal, in 2006, and received M. Tech [CSE] from JNTUH in 2008. Presently he is pursuing Ph.D. from GITAM University. He has 9 years of teaching experience in various colleges at different levels. His research interests include fluid flow in porous media, heat and mass transfer, fluid dynamics and magnetohydrodynamics, and boundary value problems. He has published four research papers in internationally reputed journals in Mathematics and Computer Science.

Please cite this article in press as: Sheri SR, Thumma T, Numerical study of heat transfer enhancement in MHD free convection flow over vertical plate utilizing nanofluids, Ain Shams Eng J (2016), http://dx.doi.org/10.1016/j.asej.2016.06.015